



Substrate-Assisted Visualization of Surfactant Micelles via Transmission Electron Microscopy

Zekun Zhang, Kaitao Li, Rui Tian* and Chao Lu*

State Key Laboratory of Chemical Resource Engineering, Beijing University of Chemical Technology, Beijing, China

OPEN ACCESS

Edited by:

Huangxian Ju,
Nanjing University, China

Reviewed by:

Chih-Ching Huang,
National Taiwan Ocean
University, Taiwan
Xia Guan,
Louisiana State University,
United States

*Correspondence:

Rui Tian
tianrui@mail.buct.edu.cn
Chao Lu
luchao@mail.buct.edu.cn

Specialty section:

This article was submitted to
Analytical Chemistry,
a section of the journal
Frontiers in Chemistry

Received: 06 December 2018

Accepted: 26 March 2019

Published: 11 April 2019

Citation:

Zhang Z, Li K, Tian R and Lu C (2019)
Substrate-Assisted Visualization of
Surfactant Micelles via Transmission
Electron Microscopy.
Front. Chem. 7:242.
doi: 10.3389/fchem.2019.00242

The visualization of the micellar morphological evolution for surfactant has drawn much attention due to its self-assemble ability to fold into various structures. However, the direct observation of the soft materials with low atomic number has been hampered because of the poor scattering contrast and complex staining process by the traditional transmission electron microscopy (TEM) techniques. Herein, we reported a novel strategy to the visualization of surfactant micelles with the assistance of layered double hydroxides (LDHs) via TEM. Owing to the uniformly distributed metal ions and positive charges in the LDHs, the surfactant at the micelle-water interface reacted with LDHs to form a stabilized architecture through electrostatic and hydrogen-bond interactions. The morphologies of the surfactant can be clearly observed through the surfactant-LDHs architectures, exhibiting high contrast by TEM techniques. Significantly, the micellar evolutions involving the spherical, rodlike, and wormlike shapes were successfully distinguished. Our results may provide great possibilities and inspirations for the visualization for morphology of soft matters.

Keywords: transmission electron microscopy, visualization, surfactant micelles, layered double hydroxides, morphological evolution

INTRODUCTION

Surfactant is a widely applied soft material which exhibits self-assemble ability to fold into micelles with various structures (Jain and Bates, 2003; Stano and Luisi, 2010; Liu et al., 2018). The studies of the morphology and structure for micelles have drawn increasing attention due to their great significance in biological and material science (Landsmann et al., 2010; Wang et al., 2013; Hu and Chou, 2014). Transmission electron microscopy (TEM) is a valid technique widely applied to provide morphological aspects for visualization (Jung et al., 2003; O'Reilly et al., 2005; Honda et al., 2010). However, the observation for the surfactant micelles has been hampered due to the poor scattering contrast of the constituent elements with low atomic number (Egerton, 2013; Proetto et al., 2014). Although the supplemented attachments of TEM (such as liquid-cell and cryo-TEM) can provide supports for the morphological studies, this method suffered from sophisticated operation and sampling procedure (Geng and Discher, 2005; Parent et al., 2017; Zeng et al., 2017; Creatto et al., 2018; Stawski et al., 2018; Zhao et al., 2018; Suys et al., 2019). Therefore, it is a topic of significance to realize the visualization for the morphological evolution of the micelles during the formation process.

Staining is commonly done with heavy metal oxides (e.g., OsO₄ and RuO₄) for improving TEM contrast (Trent et al., 1983; Serizawa et al., 2000; Humphrey, 2009; Aramaki et al., 2017; Xu et al., 2017; Parker et al., 2018). Unsatisfactorily, the staining process usually comes along with inhomogeneity for staining segment, which might affect the true representation of the samples (Smith and Bryg, 2006). Moreover, the toxicity of the heavy metals has largely limited the application of staining. The fact has motivated us to explore an environmentally friendly alternative to enhance the scattering contrast and assist the visualization of micelles (Claypool et al., 1997; Aso et al., 2013).

Layered double hydroxides (LDHs) are a class of 2D inorganic metallic layered materials composed of edge-sharing metal-hydroxide octahedral structure (Abellan et al., 2012; Tian et al., 2018). The versatile di- and trivalent metal cations distributed uniformly in the host layer with the tunable electropositivity derived from the trivalent metal ions (Wang and O'Hare, 2012; Tian et al., 2015). The constituent metal elements, positively-charged layers and the abundant active sites of LDHs provided great possibilities for the construction of functional composites through electrostatic interaction and hydrogen bonds (Rogez et al., 2011; Fan et al., 2014). These superiorities inspired us to explore the potential of LDHs to assist the visualization of surfactant micelles by TEM technique.

In this study, we demonstrated the visualization of surfactant micelles with the assist of LDHs via traditional TEM. An amphoteric surfactant *N*-hexadecyl-*N,N*-dimethyl-3-ammonio-1-propanesulfonate (SHDAB) with sulfonate anion in the head was employed. The functional groups at the micelle-water interface could react with LDHs to form a stabilized SHDAB@LDHs architecture by electrostatic and hydrogen-bond interactions (**Figure 1**). Owing to the capillary-compensated flow during droplet evaporation process, the LDHs nanoplates deposited at the edge of the droplet as "coffee-ring" (Deegan et al., 1997; Parneix et al., 2010; Cui et al., 2012) (**Scheme S1**). Visualization images with excellent contrast were achieved for SHDAB@LDHs architecture through TEM techniques. More importantly, the whole micellar morphological transition involving the spherical, rodlike and wormlike shapes could be effectively recognized with the continuously increased concentration of SHDAB (**Scheme S2**). The sizes of the micelles in the evolution identified with the data obtained from atomic force microscope (AFM). Therefore, it is anticipated that LDHs-assisted visualization of surfactant micelles may open new possibilities of TEM applications, especially for the soft materials.

METHODS

Materials, Reagents, and Instruments

All reagents in experiments are of analytical grade and used without further purification. NaOH, Al(NO₃)₃·9H₂O, Mg(NO₃)₂·6H₂O are purchased from Beijing Chemical Reagent Company (Beijing, China). SHDAB is purchased from Tokyo Chemical Industry Co. Ltd (Tokyo, Japan). Ultra-pure water was obtained from the Milli-Q purification system (Barnstead, CA, USA).

Surface tension measurements of the SHDAB surfactant were measured on a Force Tensiometer (K100) by the Wilhelmy plate technique (Kruss, Germany). Electrical conductivity measurements were accomplished using an EC 215 conductivity meter (Shanghai Jingmi Instrumental Co., China). The ultrasonic treatment was implemented in an ultrasonic cleaning machine (Kunshan Ultrasonic Instrument Co. Ltd., China) with the frequency of 100%. TEM images were measured by the Tecnai G²20 (FEI Company, USA) with the accelerating voltage of 200 kV. The morphological studies of the LDHs were implemented on a scanning electron microscope (SEM Hitachi S-4700). The morphology data of SHDAB micelles were acquired on AFM by the NanoScope 9.1 (Bruker, Germany) instrument. X-ray diffraction (XRD) patterns of SHDAB, LDHs and SHDAB@LDHs architectures were measured on a D8 ADVANCE X-ray diffractometer (Bruker, Germany). FT-IR spectra were performed on a Nicolet 6700 (Thermo Electron). Zeta potentials of all the samples were recorded on a Malvern Zetasizer 3000HS nanogranularity analyzer. Isothermal titration calorimeter (ITC) was employed to study the interaction between SHDAB and LDHs on a Nano ITC (TA Instruments Waters, LLC, UT). 1.0 mL SHDAB aqueous (3.69×10^{-4} mol·L⁻¹) was titrated into 0.25 mL LDHs (2.00×10^{-3} mol·L⁻¹) in the measurement which was periodically calibrated with an internal electric heater. The heats of interaction during each injection were measured by integration of each titration peak using the ORIGIN software delivered with the ITC.

Synthesis of MgAl-CO₃-LDHs

According to the reported method (Gao et al., 2017; Tian et al., 2018), the LDHs were prepared with a few modifications. A mixed salt solution of Mg(NO₃)₂·6H₂O (19.200 g, 0.075 mol) and Al(NO₃)₃·9H₂O (9.375 g, 0.025 mol) was dissolved in 150 mL water in a 250 mL flask. Subsequently, the prepared alkaline liquor of NaOH (8.000 g, 0.200 mol) was added to keep a constant pH value of 8.5. Then, the suspension was stirred for another 20 min, followed by transfer to a furnace tube at 110°C for 24 h. Finally, the precipitate was centrifuged, washed with water and stored at 4°C for further use.

Preparation of Surfactant Micelles

The stock solution was prepared by dissolving SHDAB (0.017 g, 0.044 mol) in 30 mL ultra-pure water. Then, the SHDAB solution with different concentration (0.0295 mM, 0.059 mM, 0.295 mM, 1.48 mM) was prepared. After the ultrasonic treatment at 50°C for 4 h, the micelles with different morphologies were acquired.

Synthesis of SHDAB@LDHs Architecture

Firstly, the LDHs suspensions were treated under ultrasonic to obtain a uniformly dispersed colloidal solution. Then, the as-prepared LDHs with different volumes (3.53, 7.06, 35.29, 176.45 μL) were added into the SHDAB surfactant micelles solution of different concentration (0.04 mM, 0.08 mM, 0.40 mM, 2.00 mM), respectively. Finally, the mixtures were treated under ultrasonic irradiation at 50°C for 4 h to prepare the SHDAB@LDHs architectures. In order to evaluate the morphological evolution of SHDAB micelles, *m*-SHDAB@LDHs architectures were prepared

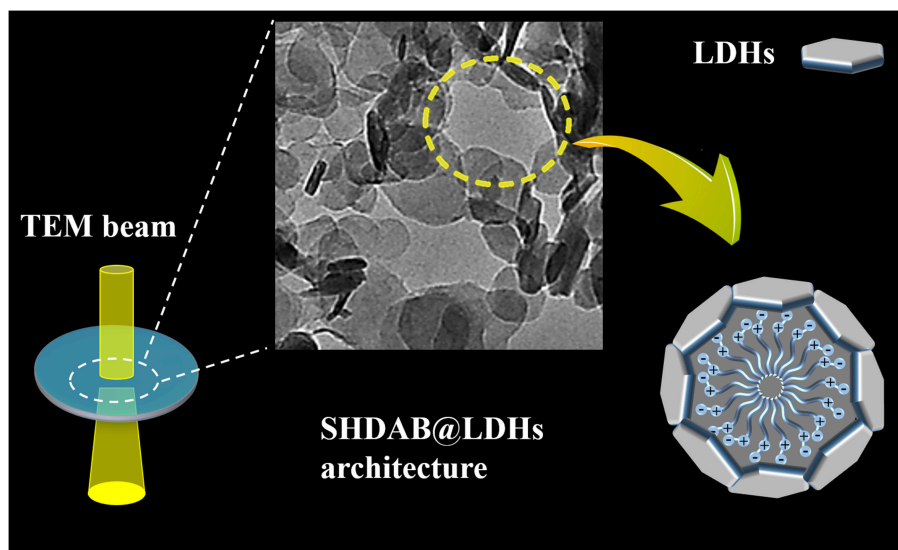


FIGURE 1 | Schematic representation of visualization for surfactant micelles with the assist of LDHs via TEM imaging.

TABLE 1 | The concentrations of SHDAB and LDHs in samples *m*-SHDAB@LDHs architectures.

Samples	SHDAB/mM	LDHs/mM
$m = 0.0295$	0.0295	0.04
$m = 0.0590$	0.0590	0.08
$m = 0.295$	0.295	0.40
$m = 1.48$	1.48	2.00

with the molecular ratio of SHDAB to LDHs determined as 0.295 to 0.400. The detailed compositions in *m*-SHDAB@LDHs architectures were listed in **Table 1**.

RESULTS AND DISCUSSION

Characterizations of the Surfactant

N-hexadecyl-*N,N*-dimethyl-3-ammonio-1-propanesulfonate (SHDAB) is a kind of betaine surfactant with negatively charged sulfonic acid in headgroup (**Figure S1**). To study the morphological transitions of SHDAB, the critical micelle concentration (CMC) has been investigated through the surface activities study (Claussen, 1967). The surface tension (γ) was plotted with the logarithm value of concentration for SHDAB. With the increased logarithm value of concentration for SHDAB, the surface tension of SHDAB decreased sharply at first and reached a relatively constant value after a marked change at 0.0295 mM for SHDAB (**Figure 2A**). The phenomenon was attributed to the presence of SHDAB monomers which preferred to adsorb at the water-air interface when the concentrations were below the CMC. When the adsorption at the water-air interface got saturated with the increased SHDAB monomers, the SHDAB tended to form micelles in the solution, exhibiting

an almost constant surface tension. The inflection point from **Figure 2A** demonstrated that the CMC of SHDAB was 0.0295 mM. Moreover, the value of CMC was also investigated by conductivity measurements (Guégan et al., 2016). **Figure 2B** showed that the conductivity (κ) grew linearly with the logarithm value of concentration for SHDAB increased. Then, a slow growth was observed when the concentration of SHDAB was larger than 0.0295 mM. Such a turning point manifested the formation of micelles was determined as CMC for SHDAB, in agreement with that obtained by surface tension measurement. Notably, the CMC value of 0.0295 mM for SHDAB accorded with previous work (Liu et al., 2013).

Visualization of Surfactant Assisted by LDHs

To observe the morphological evolution of SHDAB micelles in different concentrations, MgAl-LDHs nanoplates were prepared via a hydrothermal method (**Figure S2**) (Gao et al., 2017; Tian et al., 2018). As shown in **Figure 3A**, the LDH particles were well-dispersed after ultrasonic irradiation. High contrast of inherent LDHs can be observed, as a result of the presence of metal elements (Mg and Al) in the host layers. On the contrary, TEM image of SHDAB micelles (0.295 mM) showed the blurred boundaries on account of weak scattering contrast by the constituent light elements (**Figure 3B**). In order to distinguish the SHDAB micelles, LDH particles were added into SHDAB to construct the SHDAB@LDHs architecture for visualization. Significantly, uniformly-distributed porous structure surrounded by continuous LDHs could be observed (**Figure S3**). The reason for the formation of the porous structure may be due to the fact that the positively charged LDHs were attached at the edges of the SHDAB micelles. During the evaporation process, the LDHs nanoparticles fell apart to the edge and accumulated at the border of the SHDAB@LDHs composites, and a “coffee-ring”

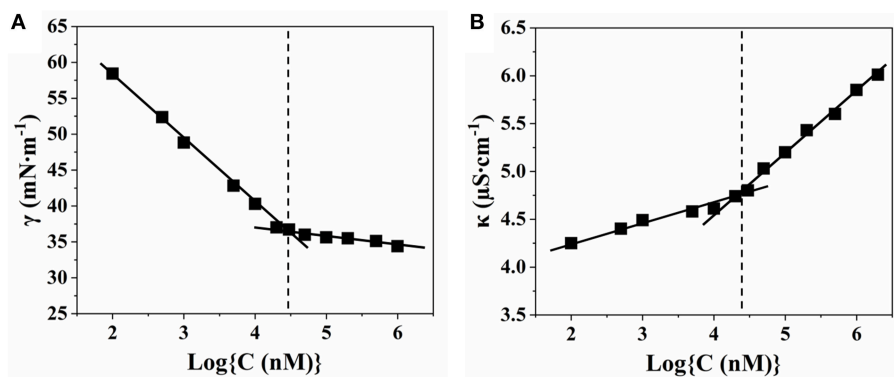


FIGURE 2 | Relationship between the concentration of SHDAB with (A) surface tension (γ) and (B) conductivity (κ), respectively.

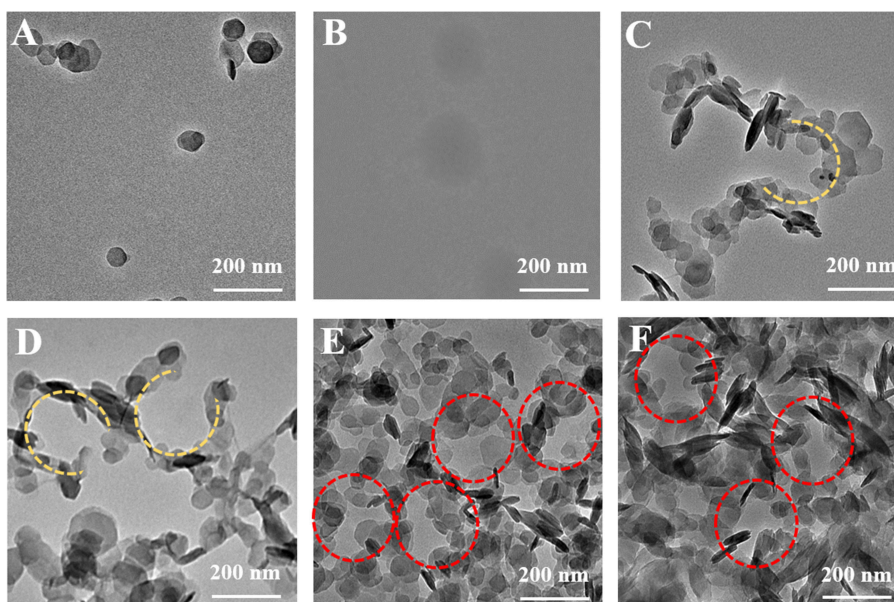


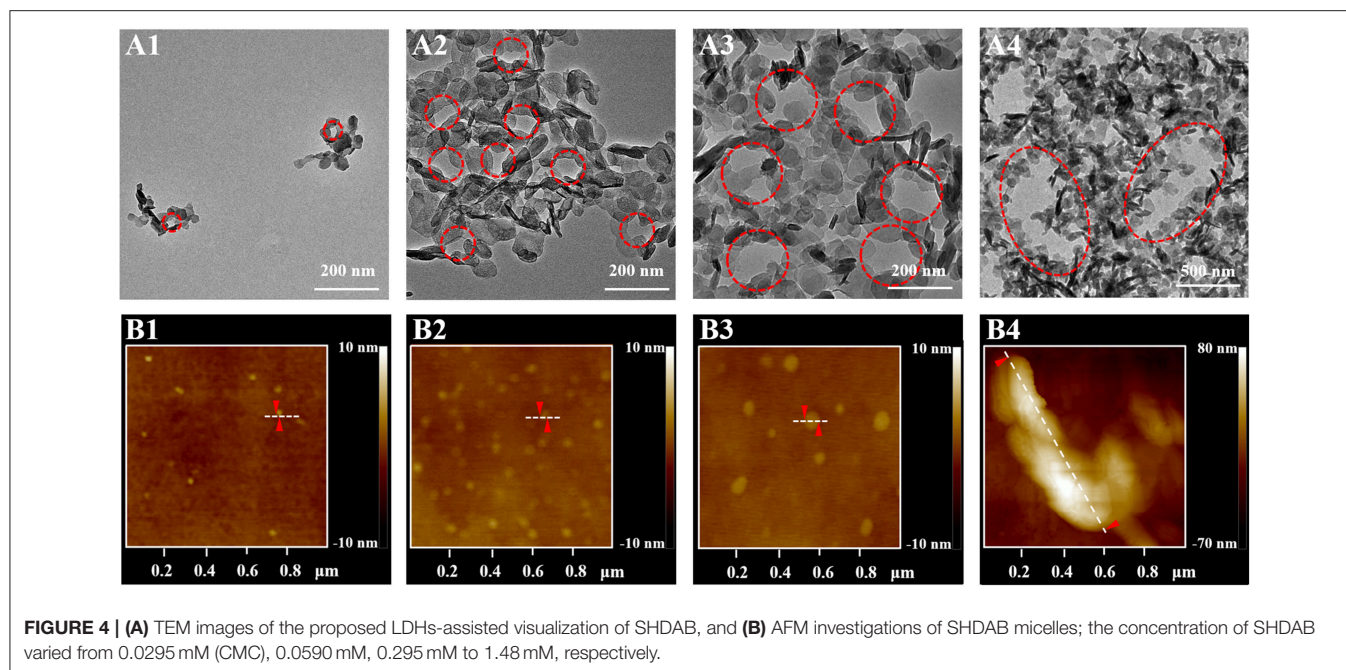
FIGURE 3 | TEM images of (A) the LDHs, (B) the SHDAB micelles and (C–F) the SHDAB@LDHs architectures with increased concentration of LDHs in SHDAB aqueous solution (0.295 mM); from C to F: 0.04 mM, 0.08 mM, 0.40 mM and 2.00 mM, respectively.

was observed (**Scheme S1**) (Deegan et al., 1997; Parneix et al., 2010; Cui et al., 2012). The results demonstrated the success of LDH-assisted visualization of SHDAB by TEM technique.

The optimum conditions for the visualization of SHDAB micelles were carried out. Firstly, the LDHs and SHDAB micelles were mixed and treated under continuous stirring. However, the LDH particles aggregated randomly (**Figure S3A**), which failed to give a description for SHDAB micelles. With the assistance of heat treatment at 50°C to accelerate the interaction, porous structures were gradually formed (**Figure S3B**). The irregular morphology indicated the insufficient combination between LDHs and SHDAB micelles. It has been reported that the ultrasonic irradiation is a powerful strategy for the improvement of the reaction efficiency due to the active energy of ultrasound waves (Hasaninejed et al., 2013). Herein, the

porous structure appeared under the condition of ultrasonic irradiation (**Figure S3C**). Moreover, heating treatment (50°C) was taken to optimize the conditions. The 0.295-SHDAB@LDHs architecture was successfully formed and stabilized with well-organized morphologies under ultrasonic irradiation along with thermal treatment (**Figure S3D**).

The quantities of LDHs in the visualization process were evaluated. LDHs with different concentrations (0.04 mM, 0.08 mM, 0.40 mM, 2.00 mM) were added into the SHDAB micelles (0.295 mM) under ultrasonic irradiation and thermal treatment. It can be observed that the LDHs nanoparticles accumulated around the SHDAB micelles gradually to form the SHDAB@LDH architecture (**Figure 3**). The porous structure was subsequently formed with the increased content of LDHs (**Figures 3C,D**), and a complete porous structures can be



formed with the LDHs content of 0.40 mM (**Figure 3E**). Moreover, the excess increase of LDHs (up to 2.00 mM) led to the aggregated LDHs overlapped with the SHDAB@LDH architecture (**Figure 3F**). Therefore, to achieve the visualization of micelles, the molecular ratio of SHDAB to LDHs was determined as 0.295 to 0.400. In addition, the time of ultrasonic irradiation also exerted an influence on the SHDAB@LDHs architectures. With the prolonged time, LDHs got adjacent to electrical double layers formed at the micelle-water interface. As depicted in **Figure S4**, the 0.295-SHDAB@LDHs architecture exhibited excellent morphology until 4 h' treatment and achieved an equilibrium state afterwards. Therefore, a finely tuned visualization strategy for micelles has been successfully established, which showed high contrast and distinguished imaging effect.

Visualization of the Morphological Evolution for the Surfactant

It has been reported that surfactants could be assembled into varied shapes when the concentrations of surfactant were larger than the CMC value (Shah et al., 2016). The SHDAB@LDHs architectures with increased concentration of SHDAB were prepared at the optimized ratio of SHDAB to LDHs (**Table 1**). With the concentration of SHDAB at the CMC value (0.0295 mM), a near-spherical porous structure was formed with an approximate radius of 26 nm, and the surfactant micelles were labeled with red dash line (**Figure 4A1**). The results indicated that the SHDAB micelles were surrounded by LDH nanoparticles. Interestingly, the porous architecture grew up to 58 nm with the concentration of SHDAB increased to 0.0590 mM (**Figure 4A2**). For the tenfold concentration of CMC value (0.295 mM), the SHDAB transformed from spherical to rodlike architecture with the size of 169 nm (**Figure 4A3**).

Moreover, closely packed LDHs nanoplates around a lanky wormlike shape (length of 879 nm) can be observed with growing concentration of SHDAB to fiftyfold concentration of CMC (1.48 mM, **Figure 4A4**). It is noteworthy that the regulated activities of SHDAB from spherical, rodlike and wormlike structures can be visualized with the assist of LDHs by TEM imaging technique.

The dimensional and morphological properties of micelles in the transition process were testified by AFM. **Figure 4B** showed the AFM profile images of the pure SHDAB in the different concentrations from one to fifty times of CMC value. It was obvious that the micelles grew up from spherical to wormlike shape along with the increased concentrations. The section analysis was implemented to acquire the size of the micelles. The micelles changed from 30 nm, 62 nm and 178 nm of spherical shape to oval with the length of 903 nm when the concentration of LDHs changed from 0.0295 mM to 1.48 mM (**Figure S5**). The AFM data were in good conformity with the TEM images assisted by LDHs (**Table S1**). Moreover, the SHDAB@LDHs architectures can also be constructed by LDHs nanoparticles with smaller size (~25 nm, **Figure S6**), and the transformation of the micelles morphology can be visualized (**Figure S7**). These results demonstrated that the size of LDHs did not influence the visualization of SHDAB, and the proposed method showed good accuracy by the assistance of LDHs.

Mechanism Studies

In order to study the mechanism for the formation of SHDAB@LDHs architectures, several experiments were carried out. As illustrated from the structure of SHDAB in **Figure S1**, the SHDAB surfactant can self-assemble into micelles by the synergetic functions of the hydrophobic interaction between

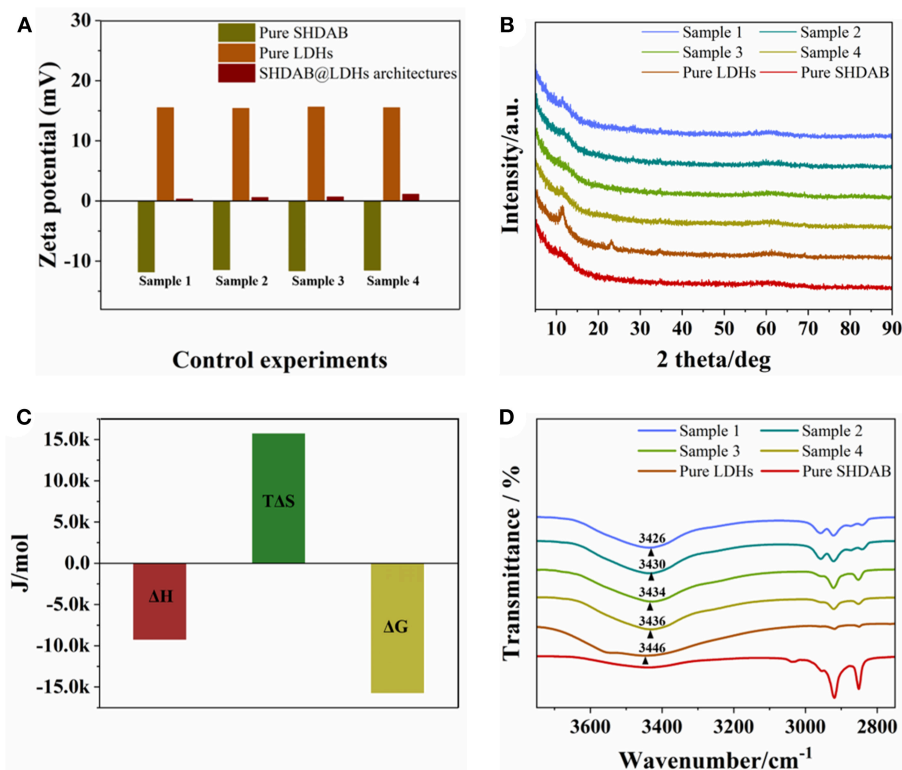


FIGURE 5 | (A) Zeta potentials, **(B)** XRD patterns, **(C)** ITC, and **(D)** FT-IR measurements of SHDAB, LDHs and SHDAB@LDHs architectures. Sample 1 to 4 represented the 0.0295-SHDAB@LDHs, 0.0590-SHDAB@LDHs, 0.295-SHDAB@LDHs and 1.48-SHDAB@LDHs architectures, respectively.

the alkane tail groups and electrostatic repulsion between the anionic head groups. As a result, the zeta potential value at the micelle-water interface of electrical double layer was -11.5 mV, indicating the stability of the SHDAB micelles with the negatively-charged groups exposed in solution (**Figure 5A**). Notably, the zeta potential of 15.5 mV for LDHs was beneficial for the electrostatic attraction toward the adjacent SHDAB micelles. The stabilized SHDAB@LDHs architecture with slight positive charge (0.3 mV) was obtained. The XRD measurements were implemented to study the structure of LDHs. The results demonstrated the unchanged interlayer space of LDHs, indicating that the SHDAB micelles were only attached at the surface of LDHs for the SHDAB@LDHs architectures (**Figure 5B**). To take a deep insight into the interaction between SHDAB micelles and LDHs, ITC measurement was carried out (**Figure S8**). The data indicated the simultaneous process for self-assembly of SHDAB micelles and the formation of the SHDAB@LDHs architectures (Kroflc et al., 2012). As shown in **Figure 5C**, the negative value of the free enthalpy showed the autonomous formation process of SHDAB@LDHs architectures (Zheng et al., 2016). Furthermore, the obvious vibration peaks in the range $3,650$ – $3,200$ cm^{-1} can be observed for the SHDAB@LDHs architectures. The peaks were blue-shifted in comparison with the FT-IR spectra for the pristine LDHs (**Figure 5D**). These results demonstrated the hydrogen bond interactions between quaternary ammonium

cations of SHDAB and hydroxyl groups of LDHs. Therefore, both electrostatic and hydrogen bond interactions contributed to the formation of SHDAB@LDHs architectures for the visualization of SHDAB.

CONCLUSION

In summary, we have presented an attractive approach for the visualization of surfactant SHDAB with the assist of LDHs via TEM imaging. Based on the electrostatic and hydrogen bond interactions between LDHs and SHDAB, well-organized SHDAB@LDHs architectures were formed. The morphologies of SHDAB surfactant can be distinguished with high scattering contrast and clear boundary, as a result of the environmentally friendly staining by LDHs. Notably, the morphological evolution involving spherical, rodlike and wormlike shapes can be witnessed, in accordance with AFM measurements. Therefore, our facile strategy opens up viable possibilities for the direct visualization of soft materials.

AUTHOR CONTRIBUTIONS

ZZ, RT, and CL conceived the experiments. ZZ and KL carried out the experiments. ZZ, RT, and CL contributed to data analysis

and writing of this manuscript. All the authors have reviewed the manuscript and agreed to its publication.

FUNDING

This work was supported by National Basic Research Program of China (973 Program, 2014CB932103), the National Natural Science Foundation of China (21656001, 21521005, 21575010

and 21701004), and Innovation and Promotion Project of Beijing University of Chemical Technology.

SUPPLEMENTARY MATERIAL

The Supplementary Material for this article can be found online at: <https://www.frontiersin.org/articles/10.3389/fchem.2019.00242/full#supplementary-material>

REFERENCES

- Abellan, G., Coronado, E., Manti-Gastaldo, C., Ribera, A., and Sanchez-Royo, J. F. (2012). Layered double hydroxide (LDH)-organic hybrids as precursors for low-temperature chemical synthesis of carbon nanoforms. *Chem. Sci.* 3, 1481–1485. doi: 10.1039/c2sc01064j
- Aramaki, K., Iwata, C., Mata, J., Maehara, T., Aburano, D., Sakanishi, Y., et al. (2017). One-step formulation of nonionic surfactant bicelles (NSBs) by a double-tailed polyglycerol-type nonionic surfactant. *Phys. Chem. Chem. Phys.* 19, 23802–23808. doi: 10.1039/c7cp02585h
- Aso, R., Kurata, H., Namikoshi, T., Hashimoto, T., Kuo, S. W., Chang, F. C., et al. (2013). Quantitative imaging of T_g in block copolymers by low-angle annular dark-field scanning transmission electron microscopy. *Macromolecules* 46, 8589–8595. doi: 10.1021/ma4014934
- Claussen, W. F. (1967). Surface tension and surface structure of water. *Science* 156, 1226–1227. doi: 10.1126/science.156.3779.1226
- Claypool, C. L., Faglioni, F., Goddard, W. A., Gray, H. B., Lewis, N. S., and Marcus, R. A. (1997). Source of image contrast in STM images of functionalized alkanes on graphite: a systematic functional group approach. *J. Phys. Chem. B.* 101, 5978–5995. doi: 10.1021/jp9701799
- Creatto, E. J., Ceccacci, F., Mancini, G., and Sabadini, E. (2018). Effect of the hydrophobic tail of a chiral surfactant on the chirality of aggregates and on the formation of wormlike micelles. *Langmuir* 34, 13288–13295. doi: 10.1021/acs.langmuir.8b02556
- Cui, L., Zhang, J., Zhang, X., Huang, L., Wang, Z., Li, Y., et al. (2012). Suppression of the coffee ring effect by hydrosoluble polymer additives. *ACS Appl. Mater. Interfaces* 4, 2775–2780. doi: 10.1021/am300423p
- Deegan, R. D., Bakajin, O., Dupont, T. F., Huber, G., Nagel, S. R., and Witten, T. A. (1997). Capillary flow as the cause of ring stains from dried liquid drops. *Nature* 389, 827–829. doi: 10.1038/39827
- Egerton, R. F. (2013). Control of radiation damage in the TEM. *Ultramicroscopy* 127, 100–108. doi: 10.1016/j.ultramic.2012.07.006
- Fan, G. L., Li, F., Evans, D. G., and Duan, X. (2014). Catalytic applications of layered double hydroxides: recent advances and perspectives. *Chem. Soc. Rev.* 43, 7040–7066. doi: 10.1039/c4cs00160e
- Gao, R., Yan, D., Evans, D. G., and Duan, X. (2017). Layer-by-layer assembly of long-afterglow self-supporting thin films with dual-stimuli-responsive phosphorescence and antiforgery applications. *Nano Res.* 10, 3606–3617. doi: 10.1007/s12274-017-1571-x
- Geng, Y., and Discher, D. E. (2005). Hydrolytic degradation of poly(ethylene oxide)-block-polycaprolactone worm micelles. *J. Am. Chem. Soc.* 127, 12780–12781. doi: 10.1021/ja053902e
- Guégan, R., Sueyoshi, K., Anraku, S., Yamamoto, S., and Miyamoto, N. (2016). Sandwich organization of non-ionic surfactant liquid crystalline phases as induced by large inorganic K4Nb6O17 nanosheets. *Chem. Commun.* 52, 1594–1597. doi: 10.1039/c5cc08948d
- Hasaninejed, A., Kazerooni, M. R., and Zare, A. (2013). Room-temperature, catalyst-free, one-pot pseudo-five-component synthesis of 4,4-(arylmethylene)bis(3-methyl-1-phenyl-1H-pyrazol-5-ol)s under ultrasonic irradiation. *ACS Sustainable Chem. Eng.* 1, 679–684. doi: 10.1021/sc400081c
- Honda, S., Yamamoto, T., and Tezuka, Y. (2010). Topology-directed control on thermal stability: micelles formed from linear and cyclized amphiphilic block copolymers. *J. Am. Chem. Soc.* 132, 10251–10253. doi: 10.1021/ja104691j
- Hu, D., and Chou, K. C. (2014). Re-evaluating the surface tension analysis of polyelectrolyte-surfactant mixtures using phase-sensitive sum frequency generation spectroscopy. *J. Am. Chem. Soc.* 136, 15114–15117. doi: 10.1021/ja5049175
- Humphrey, C. D. (2009). Negative stain transmission electron microscopy of viruses and virus-like particles. *Microsc. Microanal.* 15, 376–377. doi: 10.1017/S1431927609094446
- Jain, S., and Bates, F. S. (2003). On the origins of morphological complexity in block copolymer surfactants. *Science* 300, 460–464. doi: 10.1126/science.1082193
- Jung, H. M., Price, K. E., and McQuade, D. T. (2003). Synthesis and characterization of cross-linked reverse micelles. *J. Am. Chem. Soc.* 125, 5351–5355. doi: 10.1021/ja0271983
- Krofcik, A., Sarac, B., and Rogac, M. B. (2012). Thermodynamic characterization of 3-[(3-cholamidopropyl)-dimethylammonium]-1-propanesulfonate (CHAPS) micellization using isothermal titration calorimetry: temperature, salt, and pH dependence. *Langmuir* 28, 10363–10371. doi: 10.1021/la302133q
- Landsmann, S., Lizandara-Pueyo, C., and Polarz, S. (2010). A new class of surfactants with multinuclear, inorganic head groups. *J. Am. Chem. Soc.* 132, 5315–5321. doi: 10.1021/ja1011178
- Liu, F., Xiao, J. W., Garamus, V. M., Almásy, L., Willumeit, R., Mu, B., et al. (2013). Interaction of the biosurfactant, surfactin with betaines in aqueous solution. *Langmuir* 29, 10648–10657. doi: 10.1021/la400683u
- Liu, H., Wang, R., Wei, J., Cheng, C., Zheng, Y., Pan, Y., et al. (2018). Conformation-directed micelle-to-vesicle transition of cholesterol-decorated polypeptide triggered by oxidation. *J. Am. Chem. Soc.* 140, 6604–6610. doi: 10.1021/jacs.8b01873
- O'Reilly, R. K., Joralemon, M. J., Wooley, K. L., and Hawker, C. J. (2005). Functionalization of micelles and shell cross-linked nanoparticles using click chemistry. *Chem. Mater.* 17, 5976–5988. doi: 10.1021/cm051047s
- Parent, L. R., Bakalis, E., Ramírez-Hernández, A., Kammeyer, J. K., Park, C., Pablo, J., et al. (2017). Directly observing micelle fusion and growth in solution by liquid-cell transmission electron microscopy. *J. Am. Chem. Soc.* 139, 17140–17151. doi: 10.1021/jacs.7b09060
- Parker, K. A., Li, Y., Eshein, A., Zhu, S., Hampton, C. M., Drummy, L. F., et al. (2018). Positive staining for improved contrast of macromolecules in transmission electron microscopy. *Microsc. Microanal.* 24, 1730–1731. doi: 10.1017/S1431927618009133
- Parneix, C., Vandoolaeghe, P., Nikolayev, V. S., Quéré, D., Li, J., and Cabane, B. (2010). Dips and rims in dried colloidal films. *Phys. Rev. Lett.* 105, 266103. doi: 10.1103/PhysRevLett.105.266103
- Proetto, M. T., Rush, A. M., Chien, M. P., Baeza, P. A., Patterson, J. P., Thompson, M. P., et al. (2014). Dynamics of soft nanomaterials captured by transmission electron microscopy in liquid water. *J. Am. Chem. Soc.* 136, 1162–1165. doi: 10.1021/ja408513m
- Rogez, G., Massobrio, C., Rabu, P., and Drillon, M. (2011). Layered hydroxide hybrid nanostructures: a route to multifunctionality. *Chem. Soc. Rev.* 40, 1031–1058. doi: 10.1039/c0cs00159g
- Serizawa, T., Takehara, S., and Akashi, M. (2000). Transmission electron microscopic study of cross-sectional morphologies of core-corona polymeric nanospheres. *Macromolecules* 33, 1759–1764. doi: 10.1021/ma9907486
- Shah, A., Shahzad, S., Munir, A., Nadagouda, M. N., Khan, G. S., Shams, D. F., et al. (2016). Micelles as soil and water decontamination agents. *Chem. Rev.* 116, 6042–6074. doi: 10.1021/acs.chemrev.6b00132
- Smith, R. W., and Bryg, V. (2006). Staining polymers for microscopical examination. *Rubber Chem. Technol.* 79, 520–540. doi: 10.5254/1.3547949

- Stano, P., and Luisi, P. L. (2010). Achievements and open questions in the self-reproduction of vesicles and synthetic minimal cells. *Chem. Commun.* 46, 3639–3653. doi: 10.1039/B913997D
- Stawski, T. M., Roncal-Herrero, T., Fernandez-Martinez, A., Matamoros-Veloz, A., Kröger, R., and Benning, L. G. (2018). “On demand” triggered crystallization of CaCO₃ from solute precursor species stabilized by the water-in-oil microemulsion. *Phys. Chem. Chem. Phys.* 20, 13825–13835. doi: 10.1039/C8CP00540K
- Suys, E. J. A., Warren, D. B., Pham, A. C., Nowell, C. J., Clulow, A. J., Benameur, H., et al. (2019). A nonionic polyethylene oxide (PEO) surfactant model: experimental and molecular dynamics studies of Kolliphor EL. *J. Pharm. Sci.* 108, 193–204. doi: 10.1016/j.xphs.2018.11.028
- Tian, R., Zhang, S. T., Li, M. W., Zhou, Y. Q., Lu, B., Yan, D. P., et al. (2015). Localization of Au nanoclusters on Layered Double Hydroxides nanosheets: confinement-induced emission enhancement and temperature-responsive luminescence. *Adv. Funct. Mater.* 25, 5006–5015. doi: 10.1002/adfm.201501433
- Tian, R., Zhong, J. P., Lu, C., and Duan, X. (2018). Hydroxyl-triggered fluorescence for location of inorganic materials in polymer-matrix composites. *Chem. Sci.* 9, 218–222. doi: 10.1039/c7sc03897f
- Trent, J. S., Scheinbeim, J. I., and Couchman, P. R. (1983). Ruthenium tetroxide staining of polymers for electron microscopy. *Macromolecules* 16, 589–598. doi: 10.1021/ma00238a021
- Wang, H. Y., Zhang, L. M., Wang, J. J., Li, Z. Y., and Zhang, S. J. (2013). The first evidence for unilamellar vesicle formation of ionic liquids in aqueous solutions. *Chem. Commun.* 49, 5222–5224. doi: 10.1039/c3cc41908h
- Wang, Q., and O’Hare, D. (2012). Recent advances in the synthesis and application of Layered Double Hydroxide (LDH) nanosheets. *Chem. Rev.* 112, 4124–4155. doi: 10.1021/cr200434v
- Xu, H., Du, N., Song, Y., Song, S., and Hou, W. (2017). Vesicles of 2-ketooctanoic acid in water. *Soft Matter* 13, 2246–2252. doi: 10.1039/c6sm02665f
- Zeng, Z. Y., Zheng, W. J., and Zheng, H. M. (2017). Visualization of colloidal nanocrystal formation and electrode-electrolyte interfaces in liquids using TEM. *Acc. Chem. Res.* 50, 1808–1817. doi: 10.1021/acs.accounts.7b00161
- Zhao, M., Gao, Z., Dai, C., Zhang, Y., Sun, X., Gao, M., et al. (2018). Investigation of active-inactive material interdigitated aggregates formed by wormlike micelles and cellulose nanofiber. *J. Phys. Chem. B.* 122, 10371–10376. doi: 10.1021/acs.jpcc.8b06440
- Zheng, Y., You, S. S., Ji, C. D., Yin, M. Z., Yang, W. T., and Shen, J. (2016). Development of an amino acid-functionalized fluorescent nanocarrier to deliver a toxin to kill insect pests. *Adv. Mater.* 28, 1375–1380. doi: 10.1002/adma.201504993

Conflict of Interest Statement: The authors declare that the research was conducted in the absence of any commercial or financial relationships that could be construed as a potential conflict of interest.

Copyright © 2019 Zhang, Li, Tian and Lu. This is an open-access article distributed under the terms of the Creative Commons Attribution License (CC BY). The use, distribution or reproduction in other forums is permitted, provided the original author(s) and the copyright owner(s) are credited and that the original publication in this journal is cited, in accordance with accepted academic practice. No use, distribution or reproduction is permitted which does not comply with these terms.